This is the manuscript of the following published article:

Published version is available in IEEE Xplore Digital Library:

http://ieeexplore.ieee.org/xpl/articleDetails.jsp?arnumber=5740348

Wireless Measurement of RFID IC Impedance

Toni Björninen, *Member, IEEE*, Mikko Lauri, Leena Ukkonen, *Member, IEEE*, Risto Ritala, Atef Z. Elsherbeni, *Fellow, IEEE* and Lauri Sydänheimo, *Member, IEEE*

Abstract— Accurate knowledge of the input impedance of an RFID IC at its wake-up power is valuable as it enables the design of a performance-optimized tag for a specific IC. However, since the IC impedance is power-dependent, few methods exist to measure it without advanced equipment. We propose and demonstrate a wireless method, based on electromagnetic simulation and threshold power measurement, applicable to fully assembled RFID tags, to determine the mounted IC's input impedance in the absorbing state including any parasitics arising from the packaging and the antenna-IC connection. The proposed method can be extended to measure the IC's input impedance in the modulating state as well.

Index Terms—Impedance measurement, Microwave radio communication, Microwave antennas, Error analysis, Monte Carlo methods

I. INTRODUCTION

Radio Frequency Identification (RFID) system is a wireless automatic identification system, where objects are tagged with transponders, consisting of an antenna and an integrated circuit (IC). Passive RFID tags scavenge energy for their operation from an incident electromagnetic field, set by the reader unit. When the on-tag IC receives sufficient power to enable its full functionality, it is able to demodulate commands from the reader and to modulate the tag's response to the antenna-mode backscattered field by switching its input impedance between two values. Most importantly, the IC's memory contains a unique identification code providing an identity for the tagged object. Battery assisted passive tags are equipped with an on-tag battery to provide energy for the IC, but they also backscatter their response to the reader only under the reader's interrogation, as do the passive tags. Active RFID tags, on the other hand, are capable of independent transmission and they can act effectively as radio transmitters [1].

Computational electromagnetics (CEM) tools are essential in design of RFID tags of any type. Towards the end of the 20th century, many efficient CEM tools have become widely available for microwave engineers and at present a common work station computer can be used to simulate various microwave devices, including antennas. In field of RFID, CEM tools have been successfully applied to design efficient, compact tag antennas [2],[3]. Tag miniaturization is motivated by the application: tags need to be seamlessly integrated into product packages and have low manufacturing costs, but at the same time sufficient power transfer between the IC and the tag antenna need to be arranged to cover the global UHF RFID frequencies from 860 MHz to 960 MHz.

Research on different size-reduction and impedance matching techniques has been carried out in the RFID context [2]–[4] and the results from the research done in a more general setting [5],[6] are also available for engineers and researcher working on RFID. However, the lack of accurate knowledge of the IC's impedance may keep the tag designer from getting the full benefit out of the applied antenna design techniques. This is true particularly in design of broadband impedance matching, which is the principal design goal in many RFID tag designs. In view of this, accurate knowledge of the tag antenna properties, provided by CEM tools or measurements is not enough, but accurate knowledge of the IC impedance is crucial for successful tag design as well.

In the absorbing impedance state, the integrated rectifier and voltage multiplications stages provide sufficient DC voltage to enable the IC's functionalities. This frontend circuitry of the IC is typically composed of capacitors, diodes and semiconductor switches, making its input impedance capacitive and frequency and power dependent [7],[8]. In addition, the packaging of the IC, as well as the tag antenna-IC connection, affect the impedance, seen from the tag antenna terminals towards the IC, making the input impedance of the IC a complex quantity as a whole [9]. The same applies to the modulating state input impedance, which together with the absorbing state input impedance, determines the modulation efficiency of the tag [10],[19].

On the product datasheets, IC manufacturers typically list the input impedance of RFID ICs in the absorbing state at few frequency points in the global UHF RFID frequency band or provide an equivalent circuit model for the input impedance without presenting the actual measured impedance data. Further, the input impedance in the modulating state may not be listed at all. Thus, by measuring the chip impedance in both

operating states including the parasitic effects from the tag antenna-IC connection, uncertainty related to the conjugate impedance matching between the tag antenna and the IC can be significantly reduced and more insight to the efficiency of the backscattering modulation process can be obtained. We expect the latter to become increasingly important for passive tag design in the future as the sensitivities of the ICs improve and especially for battery assisted RFID where the on-tag power supply enables significantly better sensitivities to begin with.

If the power loss due to the impedance mismatch between the tag antenna and the IC is small enough, the IC may remain operational at any available incident power above its sensitivity level. Thus, the complex conjugate of the IC's input impedance at the sensitivity level is commonly taken as the target for the tag antenna design. In practice the input impedance of an RFID IC has a strong dependence on the incident power and therefore carrying out the impedance measurement at an appropriate incident power to the IC is of great importance [11].

Typical measurement configurations to determine the IC's input impedance include an RFID tester to determine the threshold power and a vector network analyzer (VNA) for measuring the impedance of the IC [12]. The frequency dependent threshold power of the IC is first determined with the RFID tester and the impedance is then measured at this power. The input impedance of the IC is capacitive and varies significantly from the typical 50-Ω characteristic impedance of measurement devices. This is problematic since the sensitivity of VNAs is best around their characteristic impedance with performance decaying rapidly with loads differing from the characteristic impedance [13]. By using static pre-matching [14], VNA measurements are more accurate and the incident power on the IC can be adjusted easily. Direct measurement of the input impedance of the bare IC has the disadvantage that the result does not include the effect of mounting parasitics. This can be alleviated by mounting the IC on a sample of the antenna material [12] or by employing a method for verifying the matching condition between the antenna and IC [15] specifically suitable for assembled RFID tags.

In this article, we propose a wireless measurement method for measuring the absorbing state input impedance of an IC mounted on an RFID tag, by combining information from CEM simulations and far field measurement while communicating with the tag using the EPC Gen2 protocol. The method requires few specialized measurement devices and it can be extended to measure the modulating state input impedance as well.

The rest of the article is organized as follows. Section II introduces the theoretical background and formulation of the measurement method. In Section III the design of the test tag antennas is discussed and the related simulation results, as well as the raw measurement data are presented. Section IV presents the results for the IC impedance and the uncertainties of the method, in Section V measured tag antenna performance

is compared with a prediction based on simulation with the measured IC impedance and finally conclusions are drawn in Section VI.

II. PROPOSED MEASUREMENT METHOD

A. Power Transfer between Complex Impedances

Perfect power transfer between complex source Z_S and load Z_L impedances occurs only when the impedances are complex conjugates of each other. Kurokawa studied the concept of power waves [16] and derived an expression for the ratio of the available power from the source (P_S) and the reflected power (P_R) from the load due to impedance mismatch:

$$\frac{P_R}{P_S} = \left| \frac{Z_L - Z_S^*}{Z_L + Z_S} \right|^2 = |\rho|^2, \tag{1}$$

where $(\cdot)^*$ denotes the complex conjugate. The impedance ratio, denoted by ρ in equation (1) is also defined as the power wave reflection coefficient [16]. By observing that power $P_S-P_R=P_L$ is delivered to the load, the power transmission coefficient (τ) or the matching coefficient between the source and the load can be written as

$$\tau = \frac{P_L}{P_S} = \frac{4R_S R_L}{|Z_S + Z_L|^2} = \frac{4R_S R_L}{|Z_S - (-Z_L)|^2}, \tag{2}$$

where the second equality follows from equation (1). As we assume that R_s and R_L are strictly positive, it holds that $0<\tau\leq1$ with the value $\tau=1$ being attained only under the conjugate matched condition: $Z_S=Z_L^*$ and the value $\tau=0$ being approached as the distance between Z_S and $-Z_L$ in the complex plane tends to infinity. In this study we use equation (2) to describe the quality of the power transfer between the tag antenna and the IC.

B. Threshold Power and Link Calculations for a Far Field RFID System

For far field RFID systems, the Friis' model [17] can be applied to approximate the delivered power to the IC (P_{IC}) from the generator. In the present study we use linearly polarized antennas on tag and reader side, which we have carefully aligned to minimize the link loss due to polarization mismatch and thus the Friis' model is applied assuming perfect polarization matching. Under this assumption

$$P_{IC} = \tau L_C G G_{TX} \left(\frac{\lambda}{4\pi d} \right)^2 P_{TX}, \tag{3}$$

where L_C is the cable loss factor, G_{TX} and G are the gains of the transmitter antenna and the tag antenna, respectively, P_{TX} is the time-averaged transmitted carrier power, d is the distance between the transmitter antenna and the tag antenna and τ is

the power transmission coefficient between the tag antenna and the IC.

In the absence of any multipath propagation and assuming that the receiver sensitivity is not limiting the communication with the tag, which is commonly the case with passive RFID tags, the transmitted power is given as

$$P_{TH} = \frac{P_{IC,0}}{\tau L_C G G_{TX} \left(\frac{\lambda}{4\pi d}\right)^2}, \tag{4}$$

when the delivered power to the IC equals the IC's sensitivity, denoted $P_{IC,0}$. Since in practice the sensitivity of the IC is defined with respect to an operation that produces an observable response from the tag, also P_{TH} has this property. Commonly, the sensitivity of the IC refers to its read sensitivity, i.e. to the minimum power required to reply to the EPC Gen2 protocol's *query* command. This is the most common and expectedly the least power consuming task for the IC, since the tag's reply to *query* consists only of its ID number. Therefore we adopt this definition for the IC's sensitivity as well.

As we measure the impedance at the read sensitivity of the IC, the measurement result can be useful for designing RFID tags with maximal readable range. However, it may not yield maximal operation range for other commands such as *write*.

In order to solve equation (4) with respect to the IC's impedance, contained implicitly in τ, all the other quantities in the equation need to be known and since the impedance is a complex quantity, a pair of equations is required to produce solutions for both real and imaginary parts. As modern CEM tools allow accurate simulation of simple antenna structures, we use three plain straight dipoles as test tags. These antennas, the simulation results and the developed procedure to obtain the IC impedance are described in the next section. In addition, we measure the gain of the transmitter antenna and use the IC's sensitivity provided by the manufacturer.

In the tag measurements, we used a compact anechoic cabinet and in order to further suppress any possible multipath propagation due to the non-idealities of the measurement environment, we have mapped P_{TH} to its free space value by multiplying the raw measurement quantity by a correction factor

$$\Lambda = \frac{L_{tot}}{L_c G_{tx} \left(\frac{\lambda}{4\pi d}\right)^2}, \tag{5}$$

where L_{tot} is the path loss, from the transmitter output to an imaginary unity-gain tag and L_c is the cable loss between the generator output and transmitter antenna. In our measurements, the quantity L_{tot}, is obtained through a calibration procedure included in the measurement equipment used. This process is based on measuring a reference tag with accurately known properties, which allows the system to calculate L_{tot}. For calibration, we used a reference tag provided by the measurement device manufacturer.

Though path loss correction by using the factor Λ can provide additional accuracy, correcting the measured P_{TH} is not in general necessary; the IC impedance can be obtained similarly through the procedure described below by assuming perfectly anechoic measurement environment. Therefore we have suppressed the factor Λ from the formulation presented, yet keeping in mind that at any point P_{TH} can be replaced by ΛP_{TH}.

C. Measurement of an RFID IC's Absorbing State Input Impedance

Proceeding with the solution of equation (4) with respect to the IC's impedance, the tag antenna and the IC impedances are denoted by $Z_A = R_A + jX_A$ and $Z_L = R_L + jX_L$, respectively. Considering the tag antenna as the source and the IC as the load and taking τ to be constant, equation (2) can be rearranged to

$$4R_A^2 \frac{1-\tau}{\tau^2} = \left(R_L - R_A \frac{2-\tau}{\tau}\right)^2 + \left(X_L - (-X_A)\right)^2, \tag{6}$$

which defines a circle in the complex plane with center point

$$P(\tau) = \left(R_A \frac{2-\tau}{\tau}, -X_A\right) \tag{7}$$

and radius

$$r(\tau) = 2R_A \frac{\sqrt{1-\tau}}{\tau}. \tag{8}$$

Thus, measuring P_{TH} for two tag antennas and solving τ for each measured tag from equation (4), substituting the measured values into equations (6)-(8) and locating the intersection points of the constant-τ circles obtained yields the solutions for the IC's impedance. However, as two circles may intersect each other at zero, one, two or an infinite number of points, care must be taken to pick the physically meaningful solution. The cases with one or infinite number of intersection points are special cases, rarely if ever arising in our measurement procedure and therefore we assume to have zero or two intersection points throughout the presented analysis. In the case with two intersection points, only one of them can represent the physical solution and if, due to measurement uncertainty or errors, the circles do not intersect, the IC's impedance cannot be determined from the data.

To pick the physical solution for the IC's impedance corresponding to one of the two intersection points of the constant τ-circles defined by equations (6)-(8), we use three test tags to obtain three pairs of equations, each producing two pairs of solutions. Three is the minimum number of tags required for identifying the physical impedance solution with
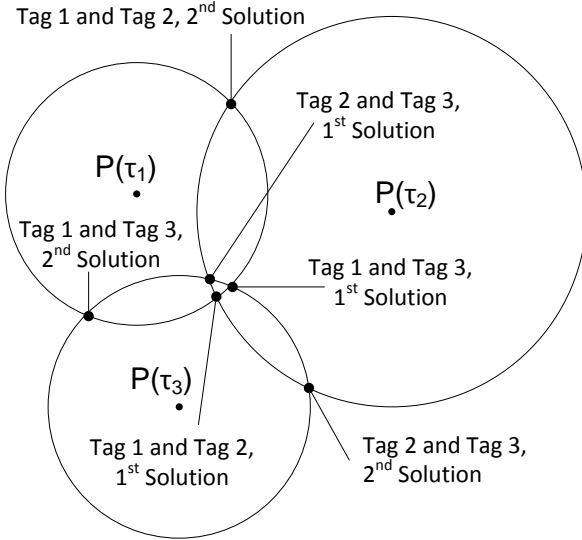
Fig. 1. Illustration of constant-τ circles obtained by measuring P_{TH} of three test tags and solutions for the IC's impedance produced by each test tag pair. The centre points and radii of the circles are determined by equations (7) and (8), respectively.

TABLE I
SOLUTION TRIPLETS WHERE ONLY ONE SOLUTION PRODUCED BY EACH TAG PAIR APPEARS.

Tag 1 and Tag 2,	Tag 1 and Tag 3,	Tag 2 and Tag 3,
1st Solution	1st Solution	1st Solution
Tag 1 and Tag 2,	Tag 1 and Tag 3,	Tag 2 and Tag 3,
1st Solution	1st Solution	2nd Solution
Tag 1 and Tag 2,	Tag 1 and Tag 3,	Tag 2 and Tag 3,
1st Solution	2nd Solution	1st Solution
Tag 1 and Tag 2,	Tag 1 and Tag 3,	Tag 2 and Tag 3,
1st Solution	2nd Solution	2nd Solution
Tag 1 and Tag 2,	Tag 1 and Tag 3,	Tag 2 and Tag 3,
2nd Solution	2nd Solution	2nd Solution
Tag 1 and Tag 2,	Tag 1 and Tag 3,	Tag 2 and Tag 3,
2nd Solution	2nd Solution	1st Solution
Tag 1 and Tag 2,	Tag 1 and Tag 3,	Tag 2 and Tag 3,
2nd Solution	1st Solution	2nd Solution
Tag 1 and Tag 2,	Tag 1 and Tag 3,	Tag 2 and Tag 3,
2nd Solution	1st Solution	1st Solution

the method described here, but using more test tags could improve the accuracy of the measurement method, since the threshold power measurement would be repeated for a greater number of individual ICs.

Assuming a sufficiently small measurement uncertainty and identical ICs in all the test tags, the physical solutions produced by each tag pair are expected to be bunched close to each other – ideally at the same point – in the complex plane, as illustrated in the Fig. 1. To identify these solutions, we consider the solution triplets (circle intersection points marked in the Fig. 1) where only one solution produced by each tag pair is included. For clarity, these triplets are listed in Table I. As we know that ideally the triangle spanned by the physical triplet would degenerate to a single point, we expect this triplet to be the three solutions on the same row in Table I, which span the triangle with the minimal circumference in the complex plane. Referring to the example in Fig. 1, this triplet would be formed by the first solutions produced by each tag pair

In this article, we only consider the case with three tags. With a number of tags $n > 3$, the selection of the physical solutions becomes more involved, since instead of triangles, n-polygons would need to be examined. As n increases, it might be useful to simply consider the sample variance of different solution combinations to determine the physical solution.

D. Measurement of an RFID IC's Modulating State Input Impedance

Assuming that the absorbing state input impedance of an IC is measured – or otherwise accurately known – the above method can be extended to extract the IC's modulating state input impedance based on the measured backscattered signal power. Below we assume that the backscattered power is measured at the transmitted threshold power, since during the backscatter measurement the incident power to the IC needs to

correspond to the value at which the absorbing state input impedance is known.

In the impedance modulation process, the input impedance of the IC is switched between the absorbing and modulating states, to modulate the response from the tag to the reader in the antenna-mode scattered field, which is the load dependent component of the total scattered field of the tag antenna [18]. The quality of this modulation procedure can be described with the modulated radar cross-section denoted as σ_m, which is analogous to the classical radar cross-section, but combines the tag antenna's reflectivity and the modulation efficiency of the tag. The total backscattered information carrying power equals the incident carrier power density at the tag's location multiplied by σ_m. Using 1:1 duty cycle in the impedance switching scheme to modulate the backscatter results in [19]

$$\sigma_m = \frac{G^2 \lambda^2}{4\pi} \frac{1}{4} |\rho_1 - \rho_2|^2, \qquad (9)$$

where ρ_1 and ρ_2 are the power wave reflection coefficients between the tag antenna and the IC in the absorbing and modulating states of the IC, respectively. Denoting the IC's impedance in the modulating state by $Z_M = R_M + X_M$, equation (9) can be written as

$$\sigma_m = \frac{G^2 \lambda^2}{4\pi} \frac{R_A^2 |Z_L - Z_M|^2}{|Z_A + Z_L|^2 |Z_A + Z_M|^2} = \frac{G^2 \lambda^2}{4\pi} L_{mod}, \qquad (10)$$

where the explicitly impedance dependent part of σ_m has been defined as the modulation loss factor L_{mod}. Under the Friis' model [17], the backscattered signal power is

$$P_{BS} = \sigma_m \frac{\lambda^2 G_{TX}^2}{(4\pi)^3 d^4} P_{TH}, \qquad (11)$$

when a single antenna with gain G_{TX} on the reader side is used for both transmission and reception. Since for a constant L_{mod}, equation (10) defines a circle in the modulating impedance plane, the intersection point method described in Section 2.3 for the absorbing state impedance can be applied for the modulating state impedance as well. In this article, we present measurement results only for the absorbing state impedance and reserve the more accurate description and demonstration of the measurement of the modulating state impedance for the future.

III. TEST TAGS AND MEASUREMENT RESULTS

The test tag antennas serve as test beds for the IC under test. From the point of view of tag antenna design, the only requirement for these antennas is sufficient gain and power matching with the IC to allow the threshold power measurement. Identical test tag antennas cannot be used, since as a result, the constant-τ circles illustrated in Fig. 1 would in theory lie on top of each other and the intersection point method described in Section II.C could not be used to find the solution for the IC's input impedance.

Keeping in mind that reliable simulation results for the test tag antennas are essential for the accuracy of the proposed method, simplistic antenna geometries are preferred. Because the measured impedance obtained from the proposed method is the input impedance of the whole circuitry beyond the test tag antenna terminals, it is important to mount the IC in the test tags exactly as in the tag antenna designs where the measured IC impedance is going to be used later.

We use straight dipole antennas to demonstrate the measurement method in practice. Dipole antennas have the advantage of structural simplicity, which facilitates accurate modeling. The dipoles are balanced structures to which ICs with differential input can be directly connected. Furthermore, dipole antennas are inherently linearly polarized, which simplifies the wireless link calculations. The size of the test tag antennas was selected so that within the studied frequency range they operate between their first and second resonance where the antenna input is inductive. This provides sufficient power matching to the IC under test to allow the threshold power measurement.

Three test tags, referred to as Tag A, Tag B, Tag C and an additional tag, Tag D were fabricated. Tag D was not used in the measurement procedure, but later to compare the measured and simulated tag antenna performance. The geometry and the dimensional parameters of all four tag antennas are shown in Fig. 2 and the values of the dimensional parameters are listed in Table II. As explained above, identical test tags cannot be used to measure the IC's impedance with the proposed method and therefore the length of each test tag antenna is different.
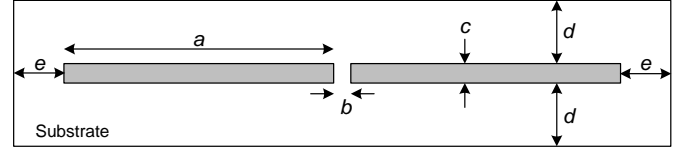

Fig. 2. Geometry and the related dimensional parameters of the test tags.

TABLE II
VALUES OF THE DIMENSIONAL PARAMETERS OF THE FABRICATED TAGS IN MILLIMETERS.

	a	b	c	d	e
Tag A	74.5	1	3	15	15
Tag B	79.5	1	3	15	15
Tag C	84.5	1	3	15	15
Tag D	89.5	1	3	15	15

TABLE III
ELECTRICAL PROPERTIES OF ROGERS RT/DUROID 5880.

Thickness	Relative permittivity	Loss tangent	Conductor material	Conductor thickness
3.17 mm	2.2	0.0009	Copper	35 μm

The assembled tags are equipped with the Alien Higgs-3 IC [20], which is provided by the manufacturer in a strap for easy attachment. Conductive epoxy was used to attach the strap to the antenna. Substrate material used for all fabricated tag antennas is the commercially available Rogers RT/Duroid 5880 with electrical properties listed in Table III.

The test tag antennas were simulated with the Ansoft High Frequency Structure Simulator (HFSS) based on the finite element method and a finite-difference time-domain (FDTD) code based on [21]. Simulated antenna impedance and gain in the direction normal to the antenna plane and away from the substrate are shown in Figs. 3-6. Good agreement between the results obtained by two fundamentally different CEM techniques provides additional assurance to our simulation procedures. Moreover, results from the two simulators serve as an example of the impact of small deviations in the simulated parameters to the final outcome of the proposed impedance measurement method.

The difference between the simulated impedance and gain between the different tag antennas is explained by the different length of the antennas alone, since all the other dimensional parameters are the same for all tags.

The threshold power of each test tag was measured in a compact anechoic cabinet with Tagformance measurement device [22], which is a measurement unit for RFID tag performance characterization. It allows power ramping at a defined frequency and thereby threshold power analysis. The
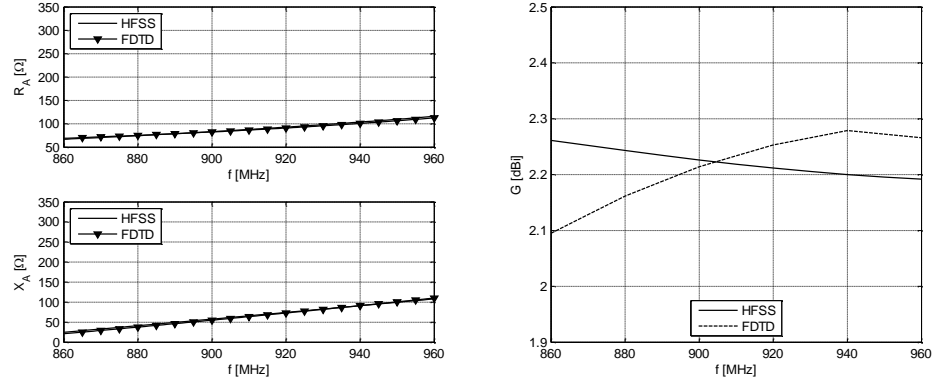
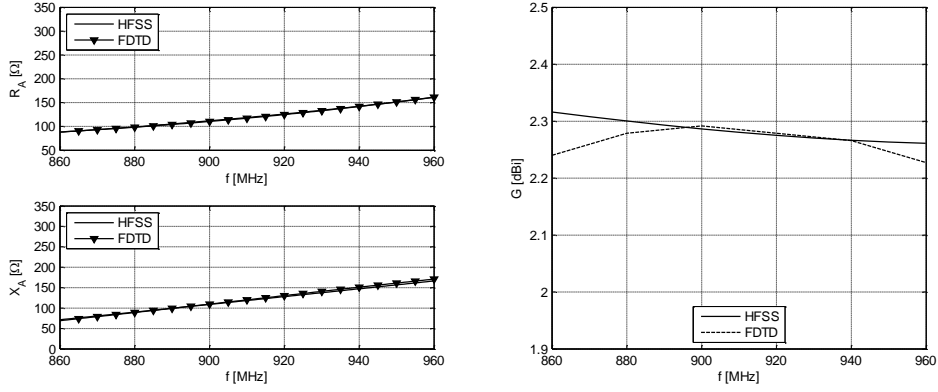Fig. 3. Simulated impedance and gain of Tag A.

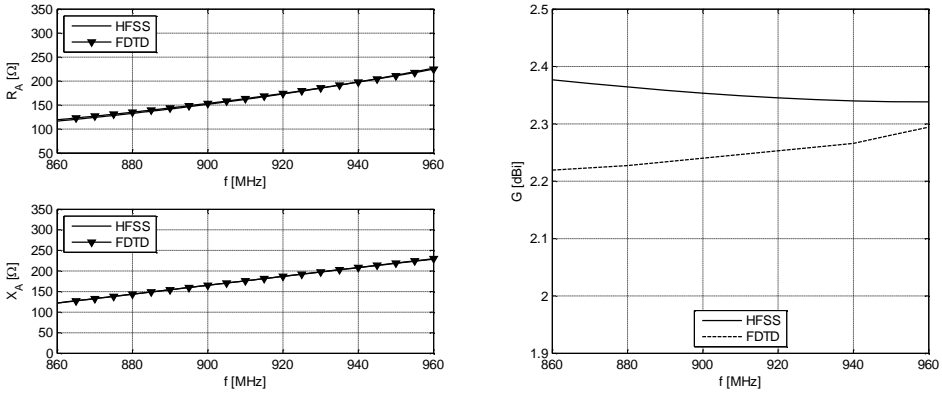Fig. 4. Simulated impedance and gain of Tag B.

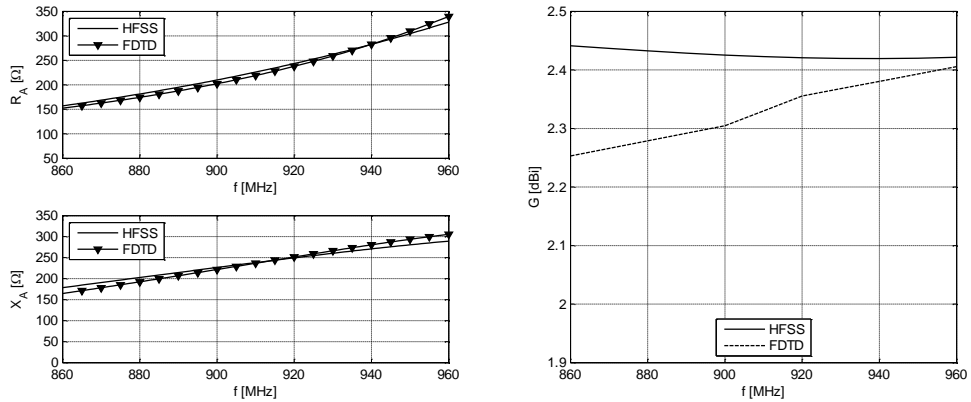Fig. 5. Simulated impedance and gain of Tag C.

Fig. 6. Simulated impedance and gain of Tag D.

core operations of the device are performed with a vector signal analyzer. The sample mean of five threshold sweeps for each individual tag in identical conditions is presented in Fig. 7. In the measurement configuration, the separation between the linearly polarized transmitter antenna and the tag under test was 0.45 m and the transmitter antenna gain, provided by the manufacturer, is shown in Fig. 8

The measured threshold power of each test tag, shown in Fig. 7, is the raw measurement data for the proposed impedance measurement method. Each curve carries information about the tag antenna gain and impedance matching, which affect the power delivery from the incident wave to the IC. For example, the transmitted threshold power of Tag A at 900 MHz is $P_{TH} \approx 2.9$ dBm. At this frequency, the free space attenuation factor $(\Lambda/4\pi d)^2$ under the Friis' model is approximately -24.7 dB, the simulated tag antenna gain is 2.2 dBi (Fig. 3) and the transmitter antenna gain is 8.6 dBi (Fig. 8). Summing these values shows that around -11 dBm incident power on the IC enables response from the tag to the *query*. Since the read sensitivity of the IC is -18 dBm [20], there is an around 7 dB mismatch loss, which translates to a power transmission coefficient $\tau \approx 0.2$. As observed from Fig. 7, we were also able to conduct the measurement with much higher mismatch loss, corresponding to up to 6 dBm threshold power. This highlights the fact that the threshold power of the test tags can be successfully measured although knowledge of IC impedance is not available for designing impedance matching for these tags. Despite the observed mismatch the highest transmitted power we needed in the experiment was around 6 dBm. This implies that the measurement method is suitable for larger measurement chambers as well.

IV. IC IMPEDANCE AND MEASUREMENT UNCERTAINTY

We have applied a Monte Carlo simulation method to determine the IC's impedance and to quantify its uncertainty. In order to perform the simulation, we first estimate the probability density function (pdf) for the tag antenna impedance Z_A, gain G and threshold power P_{TH}. As shown by measurements in [12] and [14], the read sensitivity of RFID

ICs is nearly constant in the bandwidth of interest and thus we take it to be constant in our simulations. As the conditions in the anechoic chamber remain constant during the threshold power measurement, we also assume the correction factor Λ defined in equation (5) to be constant.

A. Parametric pdf Estimation and the Simulation Procedure

Based on the principle of maximum entropy [23], we have chosen to represent the four quantities of interest as a vector valued random variable $\mathbf{x} = [R_A, X_A, G, P_{TH}]$, following a multivariate normal distribution $N(\mathbf{x}; \boldsymbol{\mu}, \boldsymbol{\Sigma})$ with parameters $\boldsymbol{\mu}$ and $\boldsymbol{\Sigma}$, the mean vector and covariance matrix, respectively. On any given frequency, the mean values for the impedance and gain of a tag antenna are obtained via CEM simulations. The mean value for threshold power at the IC's read sensitivity is obtained by using the measurement procedure described in Section III and computing the arithmetic mean of several repeated measurements. The elements of the covariance matrix are defined as:

$$\Sigma_{ij} = \begin{cases} \sigma_i^2 & \text{when } i = j \\ \rho_{ij}\sigma_i\sigma_j & \text{when } i \neq j, \end{cases} \quad (12)$$

where σ_i^2 is the variance of variable i and ρ_{ij} is the linear correlation coefficient between variables i and j. We assume the standard deviation (the square root of the variance) in both real and imaginary part of the tag antenna impedance and tag antenna gain to be proportional to their mean values. Mats et al. [24] studied the impedances of certain commercial tag antenna designs and found the 95% confidence limits of the real part of the impedances to be within ±10% of their mean value, but also less than 3 Ω even for antennas with a high resistive impedance. The 95% confidence limits of the imaginary part of the impedance was found to be at approximately 3% of their mean value. Additionally, they report that there is a slight positive correlation between the real and imaginary parts of the impedance. Based on this study, a standard deviation of 3% proportional to the mean value is set
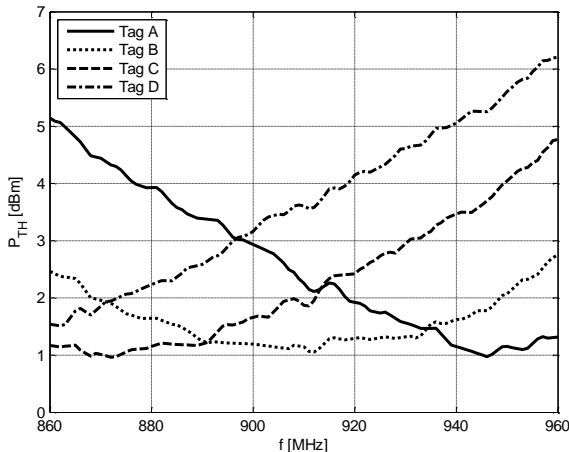

Fig. 7. Measured threshold power of the fabricated tags.
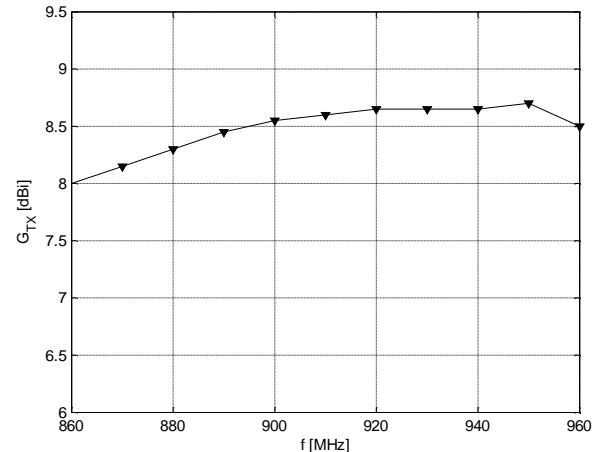

Fig. 8. Gain of the transmitter antenna.

for both the real and imaginary part of the tag antenna impedance in our test tags, with an additional limitation that the standard deviation is not allowed to be lower than 0.5 Ω or higher than 10 Ω. A weak linear correlation coefficient of 0.25 between the real and imaginary part is assumed. Additionally, based on authors' experience, the tag antenna gain is assumed to have a proportional standard deviation of 2% of its mean value on linear scale. The standard deviation for threshold power is obtained through a standard procedure [25] as sample standard deviation from measurement data. It is different for each of the tags and frequencies measured, with typical values of standard deviation ranging from 1 to 2 percent of the sample mean of the measurement result. For each of the k 𝒌 tags measured, we now have frequency dependent parametric pdf estimates $N(\mathbf{x}_k; \boldsymbol{\mu}_k(f), \boldsymbol{\Sigma}_k(f))$.

For the purposes of our simulation, we handle the complex-valued IC impedance as a two-dimensional quantity $Z_L = (R_L, X_L)$. The simulation procedure we have used is summarized in Table IV. On each measured frequency, we draw samples from the pdf estimates and compute for each possible tag pair the sample mean $Z_{ma}(f)$, which gives the expected values of IC impedance, and the sample covariance matrix $\mathbf{C}_m(f)$ to quantify the uncertainty associated with the expected values. In our simulation studies we have used a sample size of S=30000. The method described in Section 2.3, involving a search through all possible solution triplets to identify the physical solution as the triplet spanning the triangle with the minimal circumference in the complex plane is applied to select the most probable solutions for the IC impedance.

Propagating a sample from a normal distribution through the non-linear equations in Section II, results in a non-normal distribution for the IC impedance Z_L [25]. However, as in our studies no significant difference was found between representing Z_L as a normal distribution or with a more complex parametric pdf estimate, such as a Gaussian mixture model (GMM) [23], we shall only consider the normal distribution representation.

B. Impedance Measurement Results

Following the simulation procedure presented in the previous subsection, we compute for both HFSS and FDTD simulation data the sample means and sample standard deviations of each of the selected solution triplets. The results are shown in Figures 9-12.

On each frequency the solution triplet might come from a different row of Table I and therefore the details of the solution triplets are not listed in the figures. In all figures the mean values of the triplets are represented by opaque markers and the corresponding standard deviations are represented by bars.

Figures 9-10 show that the frequency trend of the three resistance solutions is consistent for both simulators. Also, for both simulators, the third resistance solution seems to differ approximately 3 Ω from the other solutions at the lowest measured frequency, but approaches the two other solutions as

TABLE IV
THE SIMULATION PROCEDURE APPLIED TO ESTIMATE IC IMPEDANCE SOLUTIONS.

1:	For each measured frequency f
2:	For each measured tag k
3:	Draw a random sample $X_{f,k}$ of size S from $N(\mathbf{x}_k; \mu_k(f), \Sigma_k(f))$.
4:	End
5:	For each possible tag combination m
6:	Applying the equations in section II, compute the IC impedances Z_m
7:	Compute sample mean $Z_{ma}(f)$ and sample covariance $C_m(f)$ of the two solutions in Z_m.
8:	End
9:	For each possible solution triplet (see Table 1 for list of all triplets)
10:	Using impedance values from all Z_m, apply the method described in section II to find the most probable solution triplet. Record the sample means and covariances for the selected triplet.
11:	End
12:	End

the frequency increases. From Figs. 11-12 it is seen that for both simulators, the frequency trends are different among the three reactance solutions. The slightly better agreement between the reactance solutions from the different simulators in the middle of the frequency band may be explained by the better agreement of the simulated gains between the different simulators at these frequencies. Also the individual characteristics of the ICs on the test tags may cause variations among the three solutions obtained using the same simulator.

At each frequency the simulation procedure of Table IV was applied to estimate the parameters of three conditional probability distributions $f_i(Z_L|Y_i)$, where Y_i are the data sets containing all measurement and simulation data related to one row of Table I, indicating the most probable solution triplet. Since on each row of Table I, each tag is present in multiple columns, we can conclude that the data sets Y_i are not independent, from which it follows that the three $f_i(Z_L|Y_i)$ are not independent. To obtain a single mean and covariance parameter on each frequency, we approximate the distributions as independent and apply Bayes' formula [23] to obtain an estimate $g(Z_L|Y_1,Y_2,Y_3)$ of the distribution of the IC's impedance given all data sets Y_i. Since all $f_i(Z_L|Y_i)$ are normal distributions with parameters $\boldsymbol{\mu}_i$ and $\boldsymbol{\Sigma}_i$, $g(Z_L|Y_1,Y_2,Y_3)$ is also a normal distribution with parameters $\boldsymbol{\mu}_t$ and $\boldsymbol{\Sigma}_t$ given by

$$\boldsymbol{\Sigma}_t^{-1} = \boldsymbol{\Sigma}_1^{-1} + \boldsymbol{\Sigma}_2^{-1} + \boldsymbol{\Sigma}_3^{-1} \tag{13}$$

$$\boldsymbol{\mu}_t = \boldsymbol{\Sigma}_t\left(\boldsymbol{\Sigma}_1^{-1}\boldsymbol{\mu}_1 + \boldsymbol{\Sigma}_2^{-1}\boldsymbol{\mu}_2 + \boldsymbol{\Sigma}_3^{-1}\boldsymbol{\mu}_3\right), \tag{14}$$
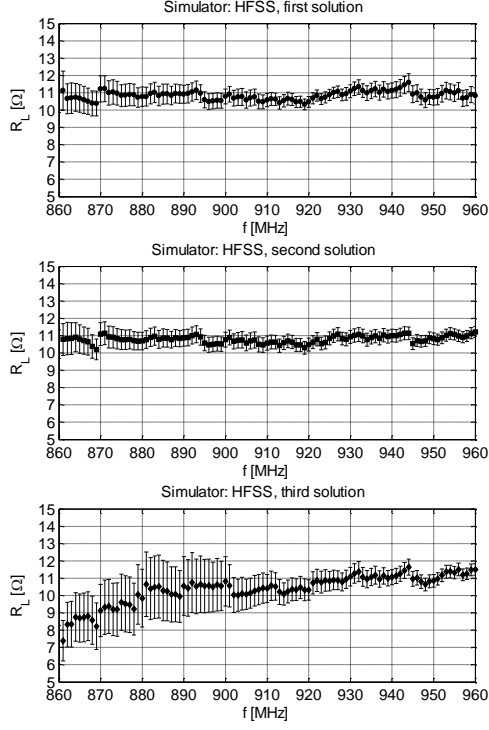
Fig. 9. Sample means with standard deviations of the IC's absorbing state input resistance using the HFSS simulation data.
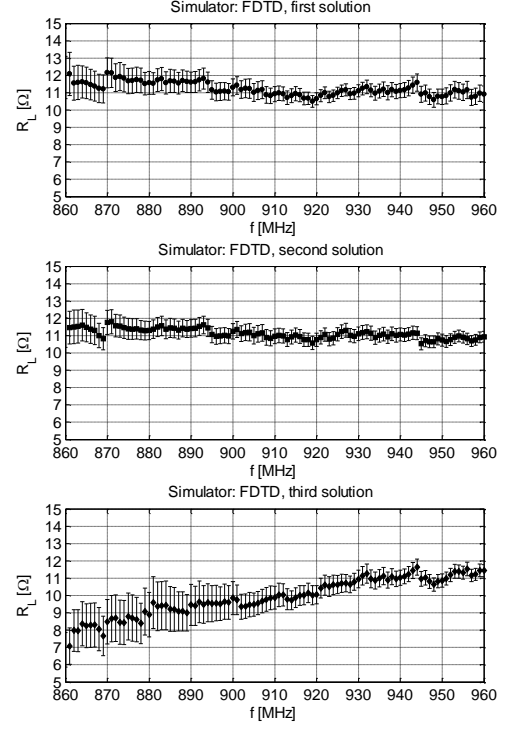

Fig. 10. Sample means with standard deviations of the IC's absorbing state input resistance using the FDTD simulation data.
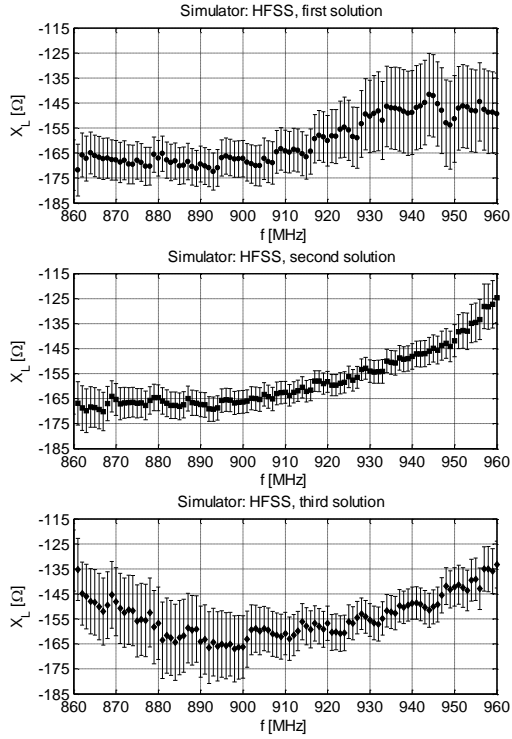

Fig. 11. Sample means with standard deviations of the IC's absorbing state input reactance using the HFSS simulation data.
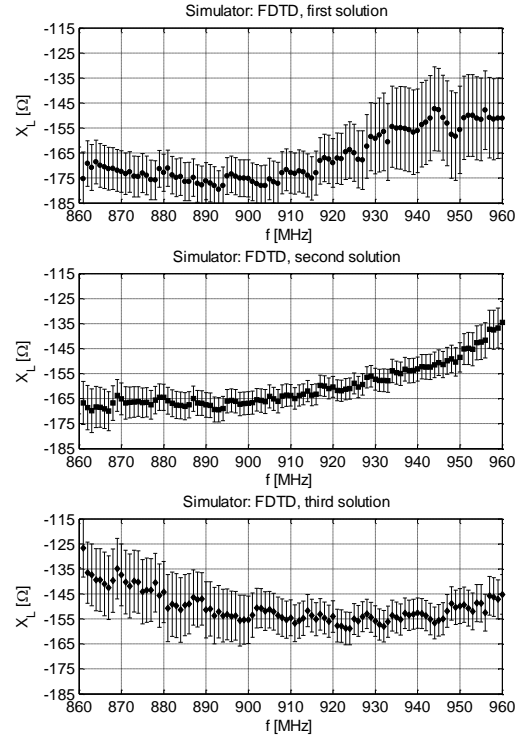

Fig. 12. Sample means with standard deviations of the IC's absorbing state input reactance using the HFSS simulation data.

where $(\cdot)^{-1}$ denotes matrix inversion. Figures 13-16 show the final estimates with one standard deviation limits for the IC's resistance and reactance with both HFSS and FDTD simulation methods. The means are indicated by opaque markers and the one standard deviation limits represented by the bars. The mean values are obtained from equation (14) and the standard deviations from equation (13).

Compared with the FDTD data, the final result with HFSS simulation data shows a steeper rise trend in the reactance after 920 MHz, but both methods predict the local reactance minimum at around 890 MHz. The standard deviations depict the uncertainty of the measured impedance and they are nearly equal using either simulation data. This suggests that the reliability of the proposed measurement method does not depend on the selected CEM tool, as long as the simulation model includes the essential physical details. The results obtained are credible from the physical point of view and indicate that our method is feasible for studying the absorbing state input impedance of an RFID IC.

It should be noted that the equivalent circuit model in the manufacturer's datasheet [20] gives somewhat different values for the input impedance of the measured IC because the circuit model is given at −14 dBm input power, whereas we measured the input impedance at the read sensitivity of the IC, which is −18 dBm. However, as a further assurance, a demonstration of the applicability of the proposed method in a practical design task is presented in the next section.
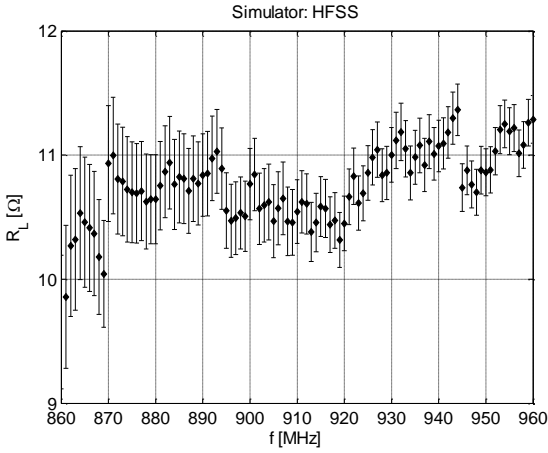

Fig. 13. Mean of the IC's absorbing state input resistance with one standard deviation bars using the HFSS simulation data.
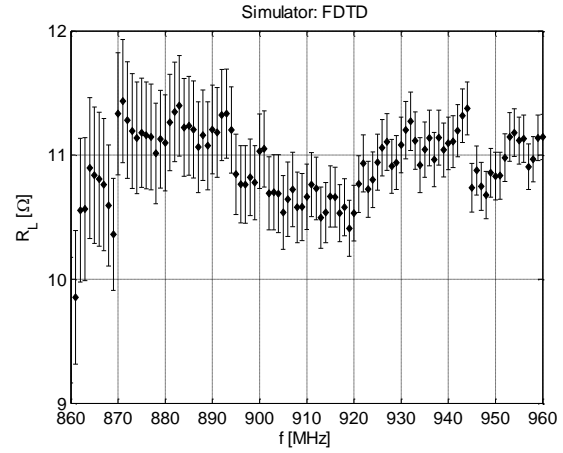

Fig. 14. Mean of the IC's absorbing state input resistance with one standard deviation bars using the FDTD simulation data.
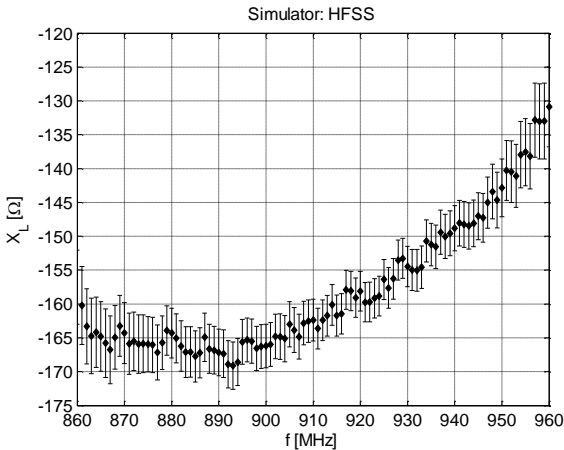

Fig. 15. Mean of the IC's absorbing state input reactance with one standard deviation bars using the HFSS simulation data.
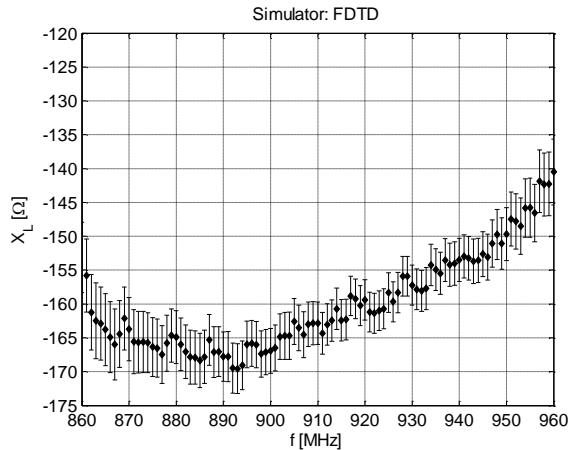

Fig. 16. Mean of the IC's absorbing state input reactance with one standard deviation bars using the FDTD simulation data.

V. DESIGN EXAMPLE USING THE MEASURED IC IMPEDANCE

For a receiving antenna, the realized antenna gain (G_R) describes how much power from an incident electromagnetic plane wave is delivered to the antenna load compared with a lossless perfectly matched isotropic antenna with identical polarization properties. In another words $G_R = G\tau$

The performance of passive RFID tags can be evaluated by analyzing the realized tag antenna gain, since currently the detection range in passive RFID systems is limited by the power delivery to the IC and G_R includes the contributions of both tag properties; the impedance matching and the tag gain, which determine the power delivery from an incident wave to the IC.

In an anechoic measurement environment, the realized gain of a tag antenna can be conveniently approximated by performing a threshold power measurement and solving equation (4) with respect to Gτ. Simulation-based estimate for realized gain is obtained in a straightforward fashion as well, provided that the IC's impedance is known. Whenever this

information is available, like in this case from the measurements, τ can be calculated according to the simulated antenna impedance using equation (2) with the antenna as the source and the IC as the load.

To evaluate the applicability of the measured IC impedance in tag antenna design we compared the measured and simulated realized gain of four tags; Tag A, Tag B, Tag C and Tag D, described in Section 3. Tag D was not used in the impedance measurement and thus it serves as an additional comparison tag, which is completely independent of the impedance measurement.

Based on the simulation results presented in Section 3, for the tag antennas considered here, the frequency trend of the realized gain is expected to be dominated by the impedance matching, due to the greater variability of the simulated tag antenna impedance and measured IC impedance compared with the simulated tag antenna gain.

Comparisons between the measured and simulated realized gains of each of the individual tag are presented in Figs. 17-20.
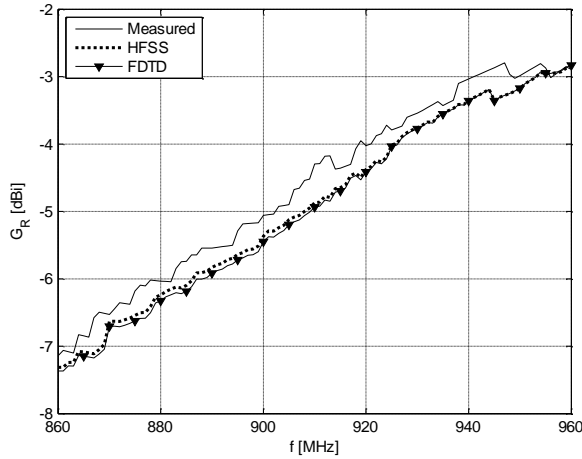

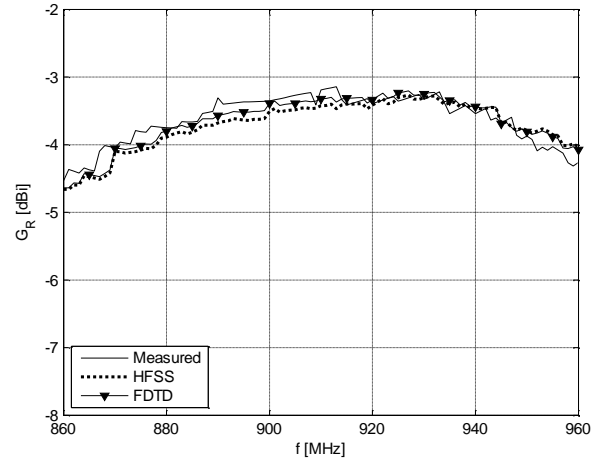Fig. 17. Measured and simulated realized gain of Tag A.

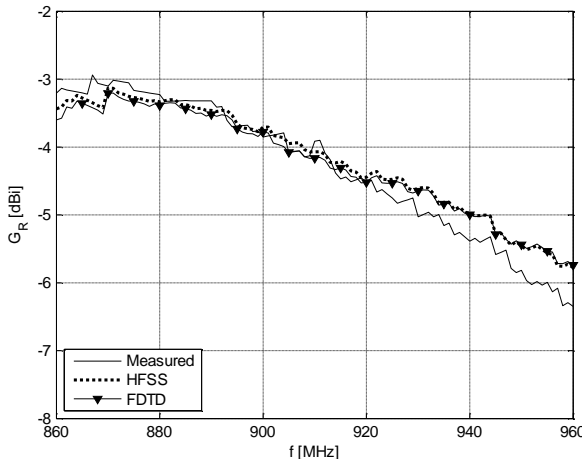Fig. 18. Measured and simulated realized gain of Tag B.

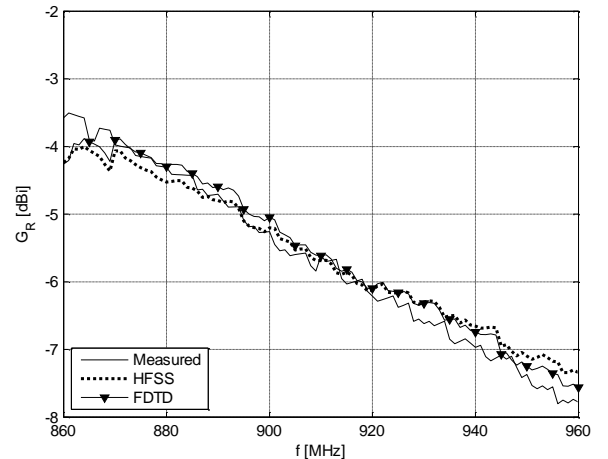Fig. 19. Measured and simulated realized gain of Tag C.

Fig. 20. Measured and simulated realized gain of Tag D.

According to the results shown in Figs. 17-20, there is a maximum 0.5 dB difference between the measured and simulated results (both simulators) for all the test tags over the studied frequency range. The frequency trend of the curves for each tag is predicted well by the simulations where the measured IC impedance was used. This suggests that the frequency dependency of the IC's impedance is captured accurately by our measurements.

As a whole the simulation and measurement results are in very close agreement, particularly for Tag B and Tag D. The slight level shift between the simulation and measurement results for Tag A and Tag C can be due to a small misalignment between the antennas during the measurement.

VI. CONCLUSIONS

We have demonstrated a wireless measurement method, based on CEM simulations and threshold power measurement, to determine the absorbing state input impedance of an RFID IC. The presented method takes into account parasitic effects arising from the packaging and the antenna-IC connection and thus provides ready-to-use data for tag antenna designers. Method has been applied to a set of test tags, its uncertainty has been quantified by Monte Carlo simulations and the simulated realized gain of the test tags using the measured IC impedance has been compared against measurement results to demonstrate the degree of accuracy expected from the proposed measurement method. Future work includes further demonstrations of the method by measuring the modulating state input impedance of an RFID IC.

REFERENCES

[1] D. Dobkin, *The RF in RFID: Passive UHF RFID in Practice*, Newline, 2008.

[2] C. Cho, H. Choo, I. Park, "Broadband RFID tag antenna with quasi-isotropic radiation pattern," *Electronics Letters*, vol. 41, no. 20, pp. 1091-1092, Sept. 2005.

[3] T. Bjorninen, L. Ukkonen, L. Sydanheimo, "Design and non-invasive design verification of a slot-type passive UHF RFID tag," *Proceedings of the 2010 IEEE Radio and Wireless Symposium (RWS)*, pp. 132-135, 10-14 Jan., 2010, New Orleans, LA, USA.

[4] G. Marrocco, "The art of UHF RFID antenna design: impedance-matching and size-reduction techniques," *IEEE Antennas Propag. Mag.*, vol. 50, no. 1, pp. 66-79, Feb. 2008.

[5] S. R. Best, J. D. Morrow, "On the significance of current vector alignment in establishing the resonant frequency of small space-filling wire antennas," *IEEE Antennas Wireless Propag. Lett.*, vol. 2, pp. 201-204, 2003.

[6] A. Harmouch, H. A. Al Sheikh, "Miniaturization of the Folded-Dipole Antenna [Antenna Designer's Notebook]," *IEEE Antennas Propag. Mag.*, vol. 51, no. 1, pp. 117-123, Feb. 2009.

[7] G. De Vita, G. Iannaccone, "Design criteria for the RF section of UHF and microwave passive RFID transponders," *IEEE Trans. Microw. Theory Tech.*, vol. 53, no. 9, pp. 2978-2990, Sept. 2005.

[8] J.-P. Curty, N. Joehl, C. Dehollain, M. J. Declercq, "Remotely powered addressable UHF RFID integrated system," *IEEE J. Solid-State Circuits*, vol. 40, no. 11, pp. 2193- 2202, Nov. 2005.

[9] J. Ryoo, J. Choo, H. Park, J. Hong, J. Lee, "Full Wave Simulation of Flip-Chip Packaging Effects on RFID Transponder," *IEEE International Conference on RFID*, vol., no., pp.37-40, 26-28 Mar. 2007.

[10] U. Karthaus, M. Fischer, "Fully integrated passive UHF RFID transponder IC with 16.7-μW minimum RF input power," *IEEE J. Solid-State Circuits*, vol. 38, no. 10, pp. 1602-1608, Oct. 2003.

[11] C.-H. Loo, K. Elmahgoub, F. Yang, A. Z. Elsherbeni, A. A. Kishk, T. Elsherbeni, L. Ukkonen, L. Sydanheimo, M. Kivikoski, S. Merilampi, P. Ruuskanen, "Chip Impedance Matching for UHF RFID Tag Antenna Design," *Progress In Electromagnetics Research, PIER 81*, 359-370, 2008.

[12] P. V. Nikitin, K. V. S. Rao, R. Martinez, S. F. Lam, "Sensitivity and Impedance Measurements of UHF RFID Chips," *IEEE Trans. Microw. Theory Tech.*, vol. 57, no. 5, pp. 1297-1302, May 2009.

[13] Agilent Technologies Inc., "Agilent Impedance Measurement Handbook. A Guide to Measurement Technology and Techniques.", 4th edition, June 2009.

[14] L. W. Mayer, A. L. Scholtz, "Sensitivity and impedance measurements on UHF RFID transponder chips," *Proceedings of The Second International EURASIP Workshop on RFID Technology*, 7-8 July, 2008, Budapest, Hungary.

[15] S.-L. Chen, K.-H. Lin, R. Mittra, "A Measurement Technique for Verifying the Match Condition of Assembled RFID Tags," *IEEE Trans. Instrum. Meas.*, vol. 59, no. 8, pp. 2123-2133, Aug. 2010.

[16] K. Kurokawa, "Power Waves and the Scattering Matrix," *IEEE Trans. Microw. Theory Tech.*, vol. 13, no. 2, pp. 194-202, Mar. 1965.

[17] H. T. Friis, "A Note on a Simple Transmission Formula," *Proc. IRE*, vol. 34, no. 5, pp. 254-256, May 1946.

[18] R. C. Hansen, "Relationships between antennas as scatterers and as radiators," *Proc. IEEE*, vol.77, no. 5, pp. 659-662, May 1989.

[19] P. Pursula, T. Vaha-Heikkila, A. Muller, D. Neculoiu, G. Konstantinidis, A. Oja, J. Tuovinen, "Millimeter-Wave Identification—A New Short-Range Radio System for Low-Power High Data-Rate Applications," *IEEE Trans. Microw. Theory Tech.*, vol.56, no.10, pp.2221-2228, Oct. 2008.

[20] Alien Technology, RFID IC datasheets: http://www.alientechnology.com/tags/rfid_ic.php.

[21] A. Z. Elsherbeni, V. Demir, *The Finite Difference Time Domain Method for Electromagnetics: With MATLAB Simulations*, SciTech Publishing, 2009.

[22] Voyantic Ltd.: http://www.voyantic.com/

[23] C. M. Bishop, *Pattern Recognition and Machine Learning*, Springer, 2006.

[24] L. Mats, J. T. Cain, M. H. Mickle, "Statistical Analysis of Transponder Packaging in UHF RFID Systems," *IEEE Trans. Electron. Packag. Manuf.*, vol. 32, no. 2, pp. 97-105, Apr. 2009.

[25] ISO GUM 95 with minor corrections, JCGM 100:2008 - Evaluation of measurement data – Guide to the expression of uncertainty in measurement. BIPM, IEC, IFCC, ILAC, ISO, IUPAC, IUPAP and OIML. 2008.